The Astrophysical Journal, 620:1010–1026, 2005 February 20

DECAY OF PLANETARY DEBRIS DISKS

G. H. Rieke,[1] K. Y. L. Su,[1] J. A. Stansberry,[1] D. Trilling,[1] G. Bryden,[2] J. Muzerolle,[1] B. White,[1] N. Gorlova,[1] E. T. Young,[1] C. A. Beichman,[3] K. R. Stapelfeldt,[2] and D. C. Hines[4]

Received 2004 August 19; accepted 2004 September 30

ABSTRACT

We report new *Spitzer* 24 μm photometry of 76 main-sequence A-type stars. We combine these results with previously reported *Spitzer* 24 μm data and 24 and 25 μm photometry from the *Infrared Space Observatory* and the *Infrared Astronomy Satellite*. The result is a sample of 266 stars with mass close to 2.5 $M_\odot$, all detected to at least the $\sim$7 σ level relative to their photospheric emission. We culled ages for the entire sample from the literature and/or estimated them using the H-R diagram and isochrones; they range from 5 to 850 Myr. We identified excess thermal emission using an internally derived $K - 24$ (or 25) μm photospheric color and then compared all stars in the sample to that color. Because we have excluded stars with strong emission lines or extended emission (associated with nearby interstellar gas), these excesses are likely to be generated by debris disks. Younger stars in the sample exhibit excess thermal emission more frequently and with higher fractional excess than do the older stars. However, as many as 50% of the younger stars do not show excess emission. The decline in the magnitude of excess emission, for those stars that show it, has a roughly t_0/time dependence, with $t_0 \sim 150$ Myr. If anything, stars in binary systems (including Algol-type stars) and λ Boo stars show less excess emission than the other members of the sample. Our results indicate that (1) there is substantial variety among debris disks, including that a significant number of stars emerge from the protoplanetary stage of evolution with little remaining disk in the 10–60 AU region and (2) in addition, it is likely that much of the dust we detect is generated episodically by collisions of large planetesimals during the planet accretion end game, and that individual events often dominate the radiometric properties of a debris system. This latter behavior agrees generally with what we know about the evolution of the solar system, and also with theoretical models of planetary system formation.

Subject headings: circumstellar matter — infrared: stars — planetary systems: formation

Online material: machine-readable table

1. INTRODUCTION

Circumstellar disks are common—perhaps ubiquitous—products of star formation. The initial steps toward planet formation must occur in the dense, often optically thick protoplanetary disks around stars less than one million years old. Such disks are dominated by primordial gas and dust, derived from the interstellar medium. These disks appear to dissipate after a few million years (e.g., Haisch et al. 2001).

It was discovered during the *Infrared Astronomy Satellite* (*IRAS*) mission (e.g., Aumann et al. 1984) that stars can still have circumstellar disks after their protoplanetary disks dissipate. Dust in these later-stage disks must be resupplied because the lifetimes for the dust grains against loss via radiation pressure, Poynting-Robertson drag, and collisional destruction are quite short (e.g., Backman & Paresce 1993; Lagrange et al. 2000; Dominik & Decin 2003). The second-generation dust in such "debris disks" is thought to arise primarily from collisions between planetesimals (asteroids) and from cometary activity and so is expected to be more plentiful in the late stages of planet formation (the "accretion end game" and "heavy bombardment" phases in the history of the solar system) than later on, when planet building is complete. This notion that the amount of dust in debris disks and its observable consequences (emission at greater than photospheric levels at mid- to far-infrared wavelengths) decline steadily over time appears to be born out by *IRAS* and *Infrared Space Observatory* (*ISO*) surveys for excess thermal emission around main-sequence stars. Such studies suggest an anticorrelation between stellar age and the magnitude of infrared excess, with timescales for the decline of the excess emission of hundreds of millions of years (e.g., Habing et al. 2001). However, neither *IRAS* nor *ISO* has been able to show unambiguously how debris-disk systems evolve, determination of which would provide clues to the development of the planetary systems that produce them. Currently, the literature contains a number of studies of evolution based on relatively small and heterogeneous samples that reach conclusions that are not totally consistent (e.g., Habing et al. 2001; Spangler et al. 2001; Laureijs et al. 2002; Decin et al. 2003; Mamajek et al. 2004; Liu et al. 2004).

Determining the evolution of debris disks has therefore been a high priority for the *Spitzer* mission. We have used the Multiband Imaging Photometer for *Spitzer* (MIPS) to observe at 24 μm a large sample of stars with masses close to 2.5 $M_\odot$ and for which we could estimate ages. We supplement the *Spitzer* sample with 25 and 24 μm data from *IRAS* and *ISO* to build a total sample of 266 stars, more than 170 of which are younger than 200 Myr. The large size, accurate photometry, and homogeneity of our sample provide a new perspective on debris disk evolution, allowing us to draw two primary conclusions: (1) there is substantial variety among debris disks, including the fact that a significant number of stars emerge from the protoplanetary stage of evolution with little remaining disk in the 10–60 AU

[1] Steward Observatory, University of Arizona, 933 North Cherry Avenue, Tucson, AZ 85721.
[2] Jet Propulsion Laboratory, 4800 Oak Grove Drive, Pasadena, CA 91109.
[3] Michelson Science Center, JPL, 4800 Oak Grove Drive, Pasadena, CA 91109.
[4] Steward Observatory. Currently at Space Science Institute, 4750 Walnut Street, Suite 205, Boulder, CO 80301.

TABLE 1

SAMPLE OF STARS

Name (1)	Object Notes (2)	K Magnitude (3)	K Reference (4)	Flux (Jy) (5)	Flux Reference (6)	Excess Ratio (7)	Age (Myr) (8)	Age Reference (9)	Type (10)	$J-K$ (11)	π (mas) (12)	$v \sin i$ km s^{-1} (13)
BD −1402022		7.86	1	0.00544	9	1.02	100	9	B5 V	−0.07	2.22	
CD −48 3524		9.70	1	0.00103	10	1.03	25	10	A2 V	0.11	2.22	
CD −48 3533		9.98	1	0.00076	10	1.00	25	10		0.15	2.22	
CD −48 3536		9.83	1	0.00094	10	1.07	25	10		0.17	2.22	
CD −48 3537		9.69	1	0.00118	10	1.18	25	10	A3 IV	0.12	2.22	
CD −48 3539		9.89	1	0.00180	10	2.16	25	10	A0	0.12	2.22	
CD −48 3540		9.02	1	0.00253	10	1.36	25	10		0.04	2.22	
CD −48 3541		9.44	1	0.00237	10	1.88	25	10		0.01	2.22	
CD −48 3558		9.85	1	0.00089	10	1.03	25	10		0.16	2.22	
CD −48 3564		9.38	1	0.00127	10	0.95	25	10	A5 IV	0.14	2.22	
CD −48 3575		10.15	1	0.00182	10	2.77	25	10		0.18	2.22	
CD −48 3578		10.18	1	0.00114	10	1.78	25	10		0.18	2.22	
CD −49 3371		9.95	1	0.00205	10	2.60	25	10		0.17	2.22	
CD −49 3390		10.28	1	0.00076	10	1.30	25	10		0.1	2.22	
CPD −48 1496		10.14	1	0.00227	10	3.43	25	10		0.13	2.22	
CPD −48 1532		10.14	1	0.00253	10	3.83	25	10		0.14	2.22	
CPD −60 944		8.65	1	0.00240	11	0.95	150	16	A0 IIp	-0.013	2.05	
CPD −60 944B		8.23	1	0.00328	11	0.88	150	16		0.006	2.05	
CPD −60 947		8.11	1	0.00402	11	0.96	150	16	A0 IIwp	-0.051	2.05	
CPD −60 948		9.17	1	0.00157	11	1.00	150	16	B8 III	0.126	2.05	
CPD −60 951		9.71	1	0.00104	11	1.10	150	16		0.072	2.05	
CPD −60 952		8.84	1	0.00207	11	0.97	150	16	A2 V	0.071	2.05	
CPD −60 954		9.22	1	0.00155	11	1.03	150	16		0.163	2.05	
CPD −60 956		9.90	1	0.00093	11	1.15	150	16	A1 V	0.21	2.05	
CPD −60 958		9.67	1	0.00106	11	1.07	150	16		0.119	2.05	
CPD −60 961		8.48	1	0.00288	11	0.97	150	16		0.043	2.05	
CPD −60 962		10.06	1	0.00072	11	1.05	150	16		0.184	2.05	
CPD −60 963		9.76	1	0.00084	11	0.93	150	16		0.1	2.05	
CPD −60 965		9.88	1	0.00100	11	1.22	150	16	A2 V	0.153	2.05	
CPD −60 972		10.09	1	0.00068	11	1.01	150	16		0.16	2.05	
CPD −60 974		9.26	1	0.00161	11	1.11	150	16	A7 III	0.122	2.05	
CPD −60 975		8.68	1	0.00391	11	1.58	150	16	A2 V	0.054	2.05	
CPD −60 977		9.38	1	0.00139	11	1.08	150	16	Avar	0.215	2.05	
CPD −60 978		8.72	1	0.00241	11	1.02	150	16		0.016	2.05	
CPD −60 981		8.94	1	0.00209	11	1.08	150	16	A7 V	0.117	2.05	
CPD −60 983		9.78	1	0.00182	11	2.03	150	16	A2 Vp	0.105	2.05	
CPD −60 984		8.99	1	0.00190	11	1.02	150	16		0.15	2.05	
CPD −60 986		9.69	1	0.00181	11	1.85	150	16	A2 V	0.046	2.05	
CPD −60 987		10.09	1	0.00059	11	0.88	150	16		0.144	2.05	
CPD −60 994		9.81	1	0.00122	11	1.40	150	16	B8.5 V	0.132	2.05	
CPD −60 996		9.84	1	0.00095	11	1.13	150	16	A8 V	0.127	2.05	
CPD −60 997		9.66	1	0.00100	11	1.00	150	16	A1 Vm	0.178	2.05	
CPD −60 1000		9.31	1	0.00123	11	0.89	150	16	A3 V	0.051	2.05	
CPD −60 1007		10.04	1	0.00118	11	1.68	150	16	A8 V	0.147	2.05	
CPD −60 1009		9.97	1	0.00067	11	0.90	150	16		0.085	2.05	

TABLE 1—*Continued*

Name (1)	Object Notes (2)	K Magnitude (3)	K Reference (4)	Flux (Jy) (5)	Flux Reference (6)	Excess Ratio (7)	Age (Myr) (8)	Age Reference (9)	Type (10)	$J-K$ (11)	π (mas) (12)	$v \sin i$ km s^{-1} (13)
CPD −60 1010		10.01	1	0.00078	11	1.08	150	16	A8 V	0.105	2.05	
CPD −60 1013		9.50	1	0.00119	11	1.02	150	16	A2 V	0.12	2.05	
CPD −60 1032		9.79	1	0.00130	11	1.47	150	16		0.101	2.05	
DAC 11A		9.83	1	0.00126	11	1.48	150	16		0.187	2.05	
DAC 79		10.59	1	0.00046	11	1.08	150	16	A0p	0.28	2.05	
DAC 81		9.75	1	0.00097	11	1.06	150	16		0.176	2.05	
DAC 227		10.21	1	0.00108	11	1.79	150	16	B8/B9	0.215	2.05	
DAC 232		10.33	1	0.00066	11	1.23	150	16	B9	0.236	2.05	
DAC 237		10.21	1	0.00063	11	1.05	150	16	F0 V	0.156	2.05	
DAC 242		10.24	1	0.00057	11	0.97	150	16	A0 V	0.198	2.05	
DAC 407		10.04	1	0.00076	11	1.08	150	16	A3 V	0.23	2.05	
DAC 516		10.20	1	0.00087	11	1.44	150	16	A0 IV–V	0.155	2.05	
DAC 624		10.10	1	0.00072	11	1.08	150	16		0.192	2.05	
DAC 704		10.23	1	0.00063	11	1.05	150	16	A0 V	0.201	2.05	
DAC 802		10.36	1	0.00055	11	1.05	150	16	A3 V	0.241	2.05	
GSC 08911−03279		9.98	1	0.00142	11	1.90	150	16		0.184	2.05	
HD 2262		3.51	2	0.422	12	1.07	690	14	A7 V	0.09	42.51	194
HD 5448		3.50	3	0.395	12	0.99	600	14	A5 V		23.93	80
HD 11636	Spectroscopic binary	2.40	2	1.12	13	1.03	620	14	A5 V	0.115	54.74	
HD 12216		3.96	3	0.315	12	1.26	320	14	A2 V		20.12	89
HD 14228	Visible double	3.86	4	0.291	12	1.07	115	14	B8 IV–V	−0.09	21.06	
HD 15008		3.96	2	0.244	12	0.98	405	14	A3 V	0.04	24.10	
HD 17573		3.82	3	0.376	12	1.32	120	14	B8 Vn		20.45	175
HD 18978		3.68	2	0.354	12	1.10	350	14	A4 V	0.11	37.85	126
HD 19356	Algol-type	2.24	3	1.87	12	1.07	300, 165	17, 14	B8 V	-0.08	35.14	55
HD 21362		5.65	1	0.324	14	8.37	80	17 (α Per)	B6 Vn	-0.03	5.89	385
HD 21364		3.90	5	0.267	12	1.01	145	14	B9 Vn	-0.03	14.68	195
HD 21981		5.59	1	0.0356	14	0.86	265	14	A1 V	0.13	8.81	118
HD 23267		6.92	1	0.0372	14	3.09	80	17 (α Per)	A0	0.017	7.33	
HD 23642	Spectroscopic binary	6.61	1	0.0223	14	1.38	125	17 (Pleiades)	A0 V	-0.037	7.60	37
HD 23753		5.59	1	0.0442	14	1.08	125	17 (Pleiades)	B8 V	-0.056	9.64	258
HD 23763		6.58	6	0.0217	14	1.32	125	17 (Pleiades)	A1 V	0.089	6.90	107
HD 23923		6.22	1	0.0495	14	2.15	125	17 (Pleiades)	B8 V	0.035	7.60	307
HD 23964	Spectroscopic binary	6.54	1	0.0200	14	1.07	125	17 (Pleiades)	A0 V	0.031	6.30	16
HD 25490		3.87	3	0.322	12	1.19	250	14	A1 V		25.24	70
HD 26321		6.80	1	0.0134	14	0.99	80	17 (α Per)	A2	0.08	5.71	
HD 27045		4.36	1	0.137	14	1.08	193, 400	17, 14	A3m		34.87	68
HD 27376	Spectroscopic binary	3.87	4	0.247	12	0.91	160	14	B9 V	−0.04	18.27	20
HD 27934		3.80	7	0.310	12	1.07	500	14	A7 IV–V		21.27	87
HD 27962		4.12	2	0.157	14	0.98	625, 320	18, 14	A2 IV	0.03	22.05	15
HD 28226		5.04	1	0.076	14	1.12	625	18	A8m	0.108	20.85	99
HD 28355		4.53	1	0.142	14	1.31	625, 520	18, 14	A7 V		20.33	
HD 28527		4.39	2	0.125	14	1.00	625, 430	18, 14	A6 IV	0.075	22.54	88
HD 29388	Visible double	3.90	1	0.189	14	0.98	625, 510	18, 14	A6 V	0.073	21.79	104
HD 30422	λ Boo–type	5.72	1	0.0469	14	1.28	10, 0	20, 14	A3 IV	−0.058	17.40	114
HD 31295	Visible double, λ Boo–type	4.42	1	0.178	14	1.46	10, 100	20, 14	A3 V		27.04	108
HD 33254	Spectroscopic binary	4.96	2	0.0761	14	1.04	625	18	A7m	0.15	18.54	17

TABLE 1—*Continued*

Name (1)	Object Notes (2)	K Magnitude (3)	K Reference (4)	Flux (Jy) (5)	Flux Reference (6)	Excess Ratio (7)	Age (Myr) (8)	Age Reference (9)	Type (10)	$J-K$ (11)	π (mas) (12)	$v \sin i$ km s^{-1} (13)
HD 33904		3.60	2	0.355	12	1.02	150	14	B9 IV	0.00	17.69	14
HD 34868		6.00	1	0.0269	14	0.96	100	19	A0 V	−0.036	7.31	97
HD 38056		6.43	1	0.0382	14	2.01	95	19	A0 V	−0.035	7.55	195
HD 38206		5.78	1	0.115	14	3.34	9	19	A0 V	0.15	14.45	30
HD 38545	λ Boo-type	5.44	1	0.0495	14	1.05	13	19	A3 Vn	0.015	7.72	183
HD 38678	ζ Lep	3.31	2	1.16	12	2.43	231, 330	17 (Pleiades), 14	A2 Vann	0.03	46.37	245
HD 39014		3.73	2	0.314	12	1.01	541, 490	17 (Pleiades), 14	A7 V	0.15	22.48	172
HD 39060	β Pic	3.49	2	8.81	12	21.9	20, 50, 100	21, 17 (Pleiades), 14	A5 V	0.1	51.87	117
HD 40183	Algol-type	1.84	2	1.62	12	0.88	350	14	A2 IV+..	−0.01	39.72	32
HD 40335		6.46	1	0.0162	14	0.88	5	14	A0	0.09	8.87	
HD 43107		5.22	1	0.0555	14	0.96	80	14	B8 V	−0.04	11.78	
HD 43378		4.33	3	0.185	12	1.04	320	14	A2 Vs		21.88	44
HD 45557		5.76	4	0.0373	14	1.06	75	19	A0 V	0.001	11.37	187
HD 46190		6.38	1	0.0239	14	1.21	5	14	A0 V	0.05	12.66	
HD 48915	Visible double	−1.38	5	34.0	13	0.95	70, 170	17 (Pleiades), 14	A1 V	−0.03	379.21	5
HD 50241		2.62	2	0.891	12	0.99	664, 615	17 (Pleiades), 14	A7 IV	0.14	32.96	206
HD 56537		3.38	3	0.586	12	1.32	560	14	A3 V		34.59	150
HD 60178	Spectroscopic binary	1.51	2	2.33	12	0.94	410	14	A2 Vm	0.02	63.27	29
HD 60856		8.00	1	0.00887	9	1.90	100	9	B5 V	−0.05	2.22	
HD 60941		8.88	1	0.00207	9	0.99	100	9	B9.5 V	0.02	2.22	
HD 60942		9.01	1	0.00200	9	1.08	100	9	B9 V	0.00	2.22	
HD 60995		8.59	1	0.00520	9	1.92	100	9	B8/B9 V	0.00	2.22	
HD 60999		8.70	1	0.00246	9	1.00	100	9	B9 V	0.00	2.22	
HD 61017		6.68	1	0.0165	9	1.05	100	9	B9 III	−0.01	2.22	
HD 61045		8.07	1	0.00440	9	1.00	100	9	B7/B8 III	−0.04	2.22	
HD 65949		8.37	1	0.00320	11	0.98	150	16		−0.04	2.05	
HD 66066A.....		7.06	1	0.0101	11	0.92	150	16	B8.5 II	−0.04	2.05	
HD 66066B.....		7.63	1	0.00547	11	0.85	150	16		−0.043	2.05	
HD 66295		8.93	1	0.00185	11	0.95	150	16	B8/B9 Ivp	0.048	2.05	
HD 66318		9.40	1	0.00118	11	0.93	150	16	Ap	0.064	2.05	
HD 68114.....		9.27	1	0.00177	10	1.20	25	10	A0 V	0.01	2.22	
HD 68115.....		9.59	1	0.00129	10	1.18	25	10	A0 V	0.01	2.22	
HD 68275		9.53	1	0.00117	10	1.01	25	10	A3m	0.1	2.22	
HD 68294		9.05	1	0.00251	10	1.39	25	10	A0 V	−0.06	2.22	
HD 68305		8.67	1	0.00263	10	1.03	25	10	A1 V	0	2.22	
HD 68398		8.45	1	0.00302	10	0.96	25	10	B9 V	0.03	2.22	
HD 68420		9.55	1	0.00328	10	2.88	25	10	A3 V	0.06	2.22	
HD 68452		9.02	1	0.00209	10	1.12	25	10		0.06	2.22	
HD 68495		9.08	1	0.00174	10	0.99	25	10	B9	0.05	2.22	
HD 68558		9.47	1	0.00178	10	1.45	25	10	A0 V	0.06	2.22	
HD 68631		9.57	1	0.00108	10	0.97	25	10	A1/A2 IV/V	0.08	2.22	
HD 68698		9.62	1	0.00212	10	1.99	25	10	A1 V	0.04	2.22	
HD 71155.....		3.92	7	0.321	14	1.54	169, 240	17 (Pleiades), 14	A0 V	−0.01	26.09	120
HD 73210		6.16	1	0.0676	14	1.01	729	22	A5 V	0.105	5.1	
HD 73666		6.53	1	0.0168	14	0.97	729	22	A1 V	−0.03	5.72	
HD 73731	Visible double	5.88	1	0.0302	14	0.96	729	22	A5m	0.061	5.95	
HD 73819		6.28	1	0.0196	14	0.90	729	22	A6 Vn	0.09	5.46	

TABLE 1—*Continued*

Name (1)	Object Notes (2)	K Magnitude (3)	K Reference (4)	Flux (Jy) (5)	Flux Reference (6)	Excess Ratio (7)	Age (Myr) (8)	Age Reference (9)	Type (10)	$J-K$ (11)	π (mas) (12)	$v \sin i$ km s^{-1} (13)
HD 73871		6.38	1	0.0184	14	0.92	729	22	A0 III	0.014	6.23	
HD 74956	Visible double	1.85	3	1.99	13	1.10	390, 330	17 (Pleiades), 14	A1 V		40.90	150
HD 75416		5.72	1	0.128	14	3.51	5	23	B8 V	0.004	10.32	
HD 76644	Spectroscopic binary	2.68	2	0.840	12	0.99	620	14	A7 V	0.09	68.32	145
HD 77327	Visible double	3.42	3	0.478	12	1.16	120	14	A1 Vne		7.71	193
HD 78045		3.75	3	0.305	12	1.00	427, 370	17 (Pleiades), 14	A2.5 IV		26.24	34
HD 79108		6.13	1	0.0477	14	1.91	320	19	A0 V	0.023	8.68	
HD 79469		3.93	3	0.332	12	1.30	180	14	B9.5 V		25.34	100
HD 80007		1.54	2	2.28	12	0.94	260	14	A2 IV	0.02	29.34	145
HD 80081	Visible double	3.51	3	0.393	12	1.04	395	14	A3 V		26.75	160
HD 80950		5.87	1	0.121	14	3.79	80	19	A0 V	0.086	12.37	40
HD 82621		4.29	3	0.190	12	1.03	285	14	A2 V		12.21	180
HD 83808	Spectroscopic binary	2.51	2	1.14	12	1.16	400	14	A5 V+	0.25	24.12	
HD 87696		4.04	2	0.299	12	1.29	390	14	A7 V	0.09	35.78	155
HD 87901		1.63	2	2.11	12	0.95	140	14	B8 Ivn	−0.06	42.09	353
HD 88955		3.73	4	0.356	12	1.15	300	14	A2 V	0.02	31.72	
HD 89021		3.37	2	0.431	12	0.96	410	14	A2 IV	0.02	24.27	35
HD 91375		4.66	1	0.107	14	1.11	265	14	A1 V	0.18	12.6	
HD 92467		6.83	1	0.0155	14	1.18	50	24	B9.5 V	0.057	7.08	
HD 92536		6.47	1	0.0488	14	2.66	50	24	B8 V	−0.021	6.80	
HD 92715		6.79	1	0.0137	14	1.01	50	24	B9.5 V	0.027	7.65	
HD 92783		6.83	1	0.0140	14	1.06	50	24	B9 V	−0.011	7.21	
HD 93540		5.57	1	0.0422	14	1.01	50	24	B6 V	−0.025	6.99	
HD 93549		5.40	1	0.0486	14	0.99	50	24	B7 IV	0.04	7.60	
HD 93738		6.35	1	0.0273	14	1.34	50	24	B9.5 V	−0.047	6.95	
HD 95370		4.09	2	0.238	12	1.07	335	14	A3 IV	0.08	15.99	86
HD 95418		2.34	2	1.40	12	1.21	300, 358, 380	25, 17 (Pleiades), 14	A1 V	0	41.07	32
HD 97603		2.26	7	0.894	15	1.01	680, 470	15, 14	A5 Ivn	0.04	56.52	173
HD 98058	Visible double	3.75	3	0.322	12	1.06	410	14	A7 Ivn		16.69	250
HD 102647		1.97	2	2.32	12	1.42	50, 520	17 (Pleiades), 14	A3 V	0.06	90.16	110
HD 103287		2.36	7	0.805	14	1.00	300, 300, 375	25, 17 (Pleiades), 14	A0 Ve	0.06	38.99	167
HD 106591		3.09	7	0.431	14	1.05	300, 335	25, 14	A3 V	0.02	40.05	
HD 108767		3.06	2	0.649	12	1.09	260	14	B9.5 V	−0.02	37.11	223
HD 109573	HR 4796A	5.77	4	3.38	12	97.2	8, 20	17 (Pleiades), 14	A0 V	0.01	14.91	152
HD 109787		3.68	7	0.350	12	1.08	330	14	A2 V	0.07	24.77	
HD 110304.....		2.14	2	1.37	12	0.99	250	14	A1 IV	−0.05	25.01	
HD 112185.....		1.75	7	1.49	14	1.05	300, 220	25, 14	A0p(var.)	−0.03	40.3	
HD 115892.....		2.70	2	0.705	14	1.20	350	14	A2 V	0.014	55.64	
HD 116842.....		3.64	2	0.331	12	0.98	300, 440	25, 14	A6 Vn	0.11	40.19	248
HD 118098.....		3.13	2	0.549	12	0.99	505	14	A3 V	0.09	44.55	178
HD 118878.....		6.34	1	0.0214	14	1.04	15	23 (U Cen)	A0 V	0.022	8.25	
HD 122408	Visible double	3.82	3	0.361	12	1.27	310	14	A3 V		14.94	15
HD 123445		6.34	1	0.0214	14	1.04	15	23 (U Cen)	B9 V	−0.035	4.57	66
HD 125162	λ Boo–type	3.91	1	0.288	14	1.49	313, 180	17 (Pleiades), 14	A3 Vp		33.58	116
HD 126135		7.08	1	0.0269	14	2.58	15	23 (U Cen)	B8 V	0.022	6.43	
HD 126997		6.43	1	0.0204	14	1.07	15	23 (U Cen)	A0/A1 V	0.186	6.92	
HD 128207		6.05	1	0.0331	14	1.23	15	23 (U Cen)	B8 V	−0.056	7.78	

TABLE 1—*Continued*

Name (1)	Object Notes (2)	K Magnitude (3)	K Reference (4)	Flux (Jy) (5)	Flux Reference (6)	Excess Ratio (7)	Age (Myr) (8)	Age Reference (9)	Type (10)	$J-K$ (11)	π (mas) (12)	$v \sin i$ km s^{-1} (13)
HD 129246	Visible double	3.64	3	0.342	12	1.02	320	14	A3 Ivn		18.07	
HD 130109		3.72	3	0.353	12	1.09	295	14	A0 V		25.35	334
HD 130697		6.48	1	0.0185	14	1.03	15	23 (U Cen)	A2 V	0.05	7.80	
HD 130841		2.43	2	1.01	12	0.95	495	14	A3 IV	0.09	42.25	80
HD 132238		6.67	1	0.0335	14	2.20	15	23 (U Cen)	B8 V	0.028	5.21	
HD 133880		5.97	1	0.0289	14	0.99	15	23 (U Cen)	B8 IV	−0.021	7.90	350
HD 133937		6.11	1	0.0243	14	0.95	15	23 (U Cen)	B7 V	−0.089	7.34	350
HD 135382		2.77	2	0.763	13	0.97	260	14	A1 V	0.1	17.85	199
HD 135454		6.83	1	0.0183	14	1.40	15	23 (U Cen)	B9 V	−0.01	7.29	
HD 135742		2.88	2	0.517	14	1.03	100, 140	17 (Pleiades), 14	B8 V	−0.05	20.38	230
HD 136246		6.96	1	0.0159	14	1.37	15	23 (U Cen)	A1 V	−0.038	6.97	
HD 136347	Visible double	6.60	1	0.0195	14	1.20	15	23 (U Cen)	A0sp	−0.014	8.10	
HD 136482		6.76	1	0.0435	14	3.09	15	23 (U Cen)	B8/B9 V	−0.068	8.03	
HD 137015	Visible double	6.86	1	0.0161	14	1.26	15	23 (U Cen)	A2 V	−0.052	6.82	
HD 138923		6.43	1	0.0595	14	3.15	15	23 (U Cen)	B8 V	−0.053	8.89	
HD 139006	Algol-type	2.20	2	1.69	12	1.29	314, 350	17 (Pleiades), 14	A0 V	0.08	43.65	132
HD 139160		6.23	1	0.0211	14	0.92	5	23	B8 IV	−0.018	5.43	130
HD 140436		3.77	3	0.237	12	0.80	160	14	B9 IV+		22.48	100
HD 141003	Visible double	3.42	5	0.439	12	1.00	300, 300	25, 14	A2 IV	0.06	21.31	200
HD 141513	Visible double	3.54	3	0.329	12	0.86	300	14	A0 V		20.94	80
HD 142105		4.12	3	0.247	12	1.15	180	14	A3 Vn		8.68	
HD 142703	λ Boo-type	5.35	1	0.0554	14	1.08	300	26	A2 Ib	0.156	18.89	102
HD 144661		6.47	1	0.0177	14	0.96	5	23	B8 IV/V	−0.016	8.50	72
HD 145964		6.39	1	0.02356	14	1.20	5	23	B9 V	−0.01	9.45	295
HD 153808	Spectroscopic binary	3.95	8	0.289	12	1.15	215	14	A0 V	−0.03	20.04	55
HD 158094	Visible double	3.84	2	0.220	12	0.80	125	14	B8 Vn	−0.05	17.42	
HD 158460		5.49	1	0.0469	14	1.05	260	14	A1 Vn	0.00	9.58	
HD 158485		6.13	1	0.0211	14	0.84	420	14	A4 V	0.03	9.15	
HD 161868		3.67	5	0.525	12	1.47	184, 305	17 (Pleiades), 14	A0 V	−0.01	34.42	212
HD 163466		6.35	1	0.0176	14	0.86	310	14	A2	0.06	5.09	
HD 164577		4.09	3	0.250	12	1.13	260	14	A2 Vn		12.31	232
HD 165459		6.60	1	0.0227	14	1.40	5	14	A2	0.05	11.2	
HD 165777	Visible double	3.43	2	0.409	12	1.01	340	14	A4 Ivs	0.06	39.40	75
HD 166014		3.67	3	0.375	12	1.15	100	14	B9.5 V		9.39	165
HD 172167	Vega	0.01	2	11.3	12	1.15	354, 365	17 (Pleiades), 14	A0 V	0	128.93	5
HD 172728		5.74	1	0.0273	14	0.77	210	14	A0 V	−0.03	7.66	
HD 178253		4.01	3	0.348	12	1.45	254, 320	17 (Pleiades), 14	A2 V		25.15	195
HD 181869		4.25	3	0.280	12	1.46	110	14	B8 V		19.20	
HD 183324	λ Boo-type	5.54	1	0.0526	14	1.22	10	20	A0 V	0.077	16.95	107
HD 184006		3.30	3	0.487	12	1.09	430	14	A5 V		26.63	210
HD 187642		0.24	2	8.06	13	1.01	700	14	A7 V	0.14	194.45	245
HD 188228		4.03	3	0.231	12	0.98	10, 20	17 (Pleiades), 14	A0 V		30.73	85
HD 192696		3.87	3	0.306	12	1.13	380	14	A3 IV–Vn		21.41	300
HD 196867	Visible double	3.89	5	0.295	12	1.11	140	14	B9 IV	−0.03	13.55	160
HD 198001		3.70	7	0.318	12	1.00	240	14	A1.5 V	0.04	14.21	105
HD 198160	Visible double, λ Boo–type	5.21	1	0.0673	14	1.15	600	20	A2.5/IV–V	0.121		
HD 202730	Visible double	3.85	3	0.292	12	1.06	400	14	A5 V		33.58	133

TABLE 1—*Continued*

Name (1)	Object Notes (2)	K Magnitude (3)	K Reference (4)	Flux (Jy) (5)	Flux Reference (6)	Excess Ratio (7)	Age (Myr) (8)	Age Reference (9)	Type (10)	$J-K$ (11)	π (mas) (12)	$v \sin i$ km s^{-1} (13)
HD 203280		1.97	2	1.707	13	1.05	820	14	A7 IV	0.15	66.84	245
HD 209952		2.10	7	0.850	14	0.83	100	14	B7 IV	−0.07	32.16	
HD 210049		4.35	4	0.176	12	1.01	245	14	A2 V	0.04	25.01	
HD 210418		3.35	2	0.464	12	1.01	450	14	A2 V	0.05	33.77	122
HD 213558	Visible double	3.71	6	0.294	13	0.94	200	14	A1 V	0.01	31.86	155
HD 214923	Visible double	3.58	2	0.398	12	1.12	120	14	B8 V	−0.05	15.64	210
HD 215789		3.28	3	0.496	12	1.02	470	14	A3 V		25.16	
HD 216956	Fomalhaut	1.01	2	4.79	12	1.21	200, 156, 480	27, 17 (Pleiades), 14	A3 V	0.05	130.08	89
HTR M25.....		10.25	1	0.00051	11	0.88	150	16		0.156	2.05	
NSV 17775		9.66	1	0.00436	10	4.23	25	10	A1 V	0.03	2.22	
P921		10.42	1	0.00070	9	1.30	100	9		0.13	2.22	
P1152		9.78	1	0.00158	9	1.62	100	9		0	2.22	
P1153		9.78	1	0.00096	9	0.98	100	9	A1 V	0.04	2.22	
P1154		9.61	1	0.00102	9	0.96	100	9	A0 V	0.02	2.22	
P1156		9.57	1	0.00121	9	1.10	100	9	A0 V	0.02	2.22	
P1157		9.34	1	0.00160	9	1.18	100	9	A0 V/B9 Vn	−0.01	2.22	200:
P1158		9.06	1	0.00224	9	1.27	100	9	A0	−0.04	2.22	
P1164		8.72	1	0.00057	9	1.07	100	9	B7/B8 III	−0.04	2.22	
P1165		8.78	1	0.00228	9	1.00	100	9	B9 V	−0.06	2.22	65
P1168		9.76	1	0.00093	9	1.00	100	9	A0 V	−0.02	2.22	
P1171		10.12	1	0.00076	9	1.07	100	9		0.07	2.22	
P1172		10.21	1	0.00113	9	1.72	100	9		0.11	2.22	
P1173		10.04	1	0.00155	9	2.03	100	9		0.05	2.22	
P1174		10.07	1	0.00058	9	0.78	100	9		0.08	2.22	
P1175		10.15	1	0.00068	9	0.97	100	9		0.09	2.22	
P1182		10.26	1	0.00114	9	1.82	100	9		0.11	2.22	
P1183		10.39	1	0.00043	9	0.78	100	9		0.16	2.22	
P1184		10.12	1	0.00068	9	0.96	100	9		0.14	2.22	
P1187		10.30	1	0.00057	9	0.95	100	9		0.16	2.22	
P1195		10.53	1	0.00053	9	1.08	100	9		0.19	2.22	
P1204		10.57	1	0.00063	9	1.34	100	9		0.19	2.22	
P1213		10.65	1	0.00041	9	0.94	100	9		0.19	2.22	
P1214		10.55	1	0.00047	9	0.97	100	9		0.2	2.22	

NOTES.—Col. (1): Star names, in alphabetical and numerical order. Col. (5): Flux density at 24 μm. Col. (7): Normalized ratio of 24 μm flux density to expected photospheric flux density. Col. (10): Spectral types from SIMBAD (see footnote 5), except HD 11636, HD 31295, HD 40183, HD 48915, HD 60178, HD 71155, HD 76644, HD 87696, HD 87901, HD 95418, HD 97603, HD 102647, HD 103287, HD 116842, HD 118098, HD 123445, HD 125162, HD 132238, HD 139006, HD 139160, HD 161868, HD 165777, HD 172167, HD 187642, and HD 203280, which are from Gray et al. (2004), and HD 27045 and HD 33254, which are from Hauck & North (1993). Column (12): Parallaxes from SIMBAD. In computing the distances of HD 123445, HD 132238, and HD 139160, a value of 6 mas was used in calculating luminosity, because it is consistent with the measured value and more in line with the moving group membership. Col. (13): from SIMBAD. Table 1 is also available in machine-readable form in the electronic edition of the *Astrophysical Journal*.

REFERENCES.—(1) 2MASS, Cutri et al. 2003; (2) Gezari et al. 2000; (3) based on visual photometry, standard colors, and *IRAS* band 1; (4) Carter 1990; (5) Selby et al. 1988; (6) Kidger & Martín-Luis 2003; (7) from SIMBAD; (8) Leggett et al. 1986; (9) MIPS, Gorlova et al. 2004; (10) MIPS, Young et al. 2004; (11) MIPS, J. Muzerolle 2004, private communication; (12) *IRAS* FSC; (13) *IRAS* Point Source Catalog; (14) MIPS, this work; (15) Laureijs et al. 2002. (16) Cameron 1985; (17) Song et al. 2001; (18) Perryman et al. 1998; (19) Gerbaldi et al. 1999; (20) Paunzen 1997; (21) Barrado y Navascués et al. 1999; (22) Bonatto et al. 2004; (23) U Sco, de Zeeuw et al. 1999; (24) IC 2602, Randich et al. 2001; (25) King et al. 2003; (26) Iliev & Barzova 1995; (27) Barrado y Navaqués et al. 1997.

region, and (2) much of the dust in these systems is generated episodically by collisions of large planetesimals and is depleted on timescales that are short compared to the age of the star.

2. THE SAMPLE

Table 1 lists the sample of stars used for this study, along with the relevant data and references. Columns (1), (3), and (5) list the stars and their K and 24 or 25 μm photometry. Column (7) shows the ratio of the measured 24 or 25 μm flux density to the flux density expected for the stellar photosphere, a ratio hereafter termed the excess ratio. Age estimates (col. [8]) are either from cluster and moving group membership or found by locating the stars on the Hertzsprung-Russell (H-R) diagram as described in the Appendix. The first estimate listed is used in our study; the other entries are for comparison purposes. Columns (10) and (11) list spectral type and $J - K$ colors. For cluster members with no spectral types, we included stars with $J - K < 0.2$, appropriate for A stars with modest reddening. Comparison with the tabulated colors of the stars in the same clusters that do have spectral types shows that this choice is appropriate (for reference, the unreddened $J - K$ values for A7, F0, and F2 dwarfs are, respectively, 0.12, 0.16, and 0.21). Column (12) lists parallaxes from *Hipparcos*, or in the case of clusters, from the adopted cluster distance (usually from main-sequence fitting), and column (13) lists the stellar rotation velocities, when they are available. References and other relevant information (e.g., whether the star is a binary) are given in columns (2), (4), (6), and (9) and in the notes to the table.

This sample was selected so that accurate measurements to the expected level of the photospheric flux densities at 24 or 25 μm are available for all members. It has 266 members within a factor of $\sim$1.5 of 2.5 $M_{\odot}$. Ages range from $\sim$5 to 850 Myr, with a good representation of all ages over this range. Through inclusion of members of young clusters, we achieve very good sampling of the young end of this age range, with more than 170 stars less than 200 Myr of age. Mature stars are also well represented, with more than 80 older than 200 Myr. To avoid contamination by gaseous emission, we have excluded all stars with strong emission-line spectra. The *Spitzer* images were inspected and seven additional stars were rejected because of extended emission that suggests that their observed excesses arise from nearby interstellar dust, rather than from debris disks.

This sample represents a substantial advance over those used for previous studies of the dependence of debris disk emission on stellar age (e.g., Habing et al. 2001; Spangler et al. 2001; Laureijs et al. 2002; Decin et al. 2003): (1) the stars are of similar mass; (2) the sample size is substantially larger; and (3) we include many stars with well-determined ages from moving group or cluster membership.

3. OBSERVATIONS

3.1. 24 μm *Spitzer Observations*

Our sample includes new 24 μm observations of 76 main-sequence, A-type stars with the MIPS instrument (Rieke et al. 2004) on *Spitzer*. All the data were collected using the photometry astronomical observing template (AOT), which is designed to provide accurate measurements on point sources. The targets in this program were selected on the basis of spectral type (generally B7 IV/V–A7 IV/V), distance ($\leq$150 pc), and cluster/moving group membership to support age estimation. For the relatively bright stars in this part of our sample, the nominal signal-to-noise ratio (S/N) approaches 100 and is limited by the intrinsic repeatability of MIPS photometry.

TABLE 2
70 μm Photometry

Name	Flux (mJy)	Error (mJy)
HD 21362	129	6
HD 71155	223	4
HD 75416	30	3
HD 125162	367	8

Notes.—Nominal noise levels are listed to demonstrate the statistical S/N. The measurements are subject to systematic calibration errors up to 20%.

We also utilize 24 μm Spitzer measurements of 111 stars in young clusters (NGC 2547, 25 Myr, from Young et al. 2004; M47, 100 Myr, from Gorlova et al. 2004; and NGC 2516, 150 Myr, from J. Muzerolle 2004, private communication). These measurements all utilized the scan map AOT, which is designed for mapping large regions but also provides excellent photometric accuracy at 24 μm because of the multiple sightings (20 in these observations) of every source. Late B-type and A-type stars were selected post facto based on $J - K$ colors. All reported photometry is for sources detected to at least the 7 σ level, but $\geq$10 σ is more typical. Further details regarding these measurements are provided by Gorlova et al. (2004) and Young et al. (2004).

The data were processed through the MIPS instrument team data analysis tool to produce calibrated, mosaicked images (Gordon et al. 2005a, 2005b). Fluxes were measured by aperture photometry, with aperture corrections determined from observed point-spread functions of calibration stars. The internal accuracy of our 24 μm photometry derived in this way is 1%–2%, although somewhat reduced accuracy (3%–5%) is achieved on objects at the flux levels of the faint members of this sample because of negative latent images and the behavior of the background surrounding them. The absolute calibration is good to 10%. The results are reported in Table 1.

3.2. *Additional Observations*

We supplemented the *Spitzer* observations with 25 μm measurements of 78 A stars from *IRAS*. We took data from both the Faint Source Catalog (FSC; Moshir et al. 1989) and the Point Source Catalog (IPAC 1986). The source of the *IRAS* photometry is indicated in Table 1; we have included only targets with high-quality measurements (*IRAS* data quality flag of 3). In general, the *IRAS* data are expected to be accurate to the 5%–10% level, depending on the source brightness and the number of passes over its position that are combined into the cataloged measurement. We used one 24 μm measurement from *ISO* (Laureijs et al. 2002), as indicated in Table 1.

Because of the relatively large beam for the *IRAS* measurements, we compared the color between the visible/near-infrared bands and *IRAS* band 1 (12 μm) with expectations for the spectral type. A number of stars appeared to be too red, and for each of these we searched the *IRAS* beam area in 2MASS to identify any sources that could contaminate the *IRAS* data. Virtually all of these cases could be explained by contaminating sources; where the sources were bright enough to affect our results, we rejected the star.

We also report four MIPS measurements of stars in our sample at 70 μm, summarized in Table 2. As with the 24 μm data, these data were reduced with the MIPS team data analysis tool (Gordon et al. 2005a, 2005b). Repeatability of the data in

this band is currently better than 5% rms, but we have not yet determined fully the necessary linearity corrections to relate measurements of sources of different brightnesses. The calibration of these measurements is therefore uncertain at a 20% level.

Near-infrared photometry was obtained from 2MASS (Cutri et al. 2003) and additional references that are given in Table 1. We used K-band photometry as the basis for extrapolating to the expected photospheric flux densities at 24 or 25 μm (see below). Where it would improve the accuracy of available K photometry, we combined measurements at J and/or H with K, assuming the normal colors for the spectral type of the star. Typical nominal errors in the K photometry are 3% rms. When K photometry is not available, we estimate a value from the visible-range photometry and standard colors, supplemented with the *IRAS* 12 μm measurement to check for any infrared anomalies.

4. AGE ESTIMATES

Ages are estimated for the sample members in three ways: (1) by association of the star with a cluster or moving group with a well-determined age; (2) when such association is not possible and the star is closer than 90 pc, by placing the star on the H-R diagram (see Appendix); or (3) by ages from the literature, mostly using Strömgren photometry (Song et al. 2001). Ages from the first method can be relatively accurate because they can draw on information for a range of stellar masses and apply it to stars whose ages are difficult to determine individually. The second method can be applied generally to any star with an accurate distance, spectral type, and photometry. When the star is near the main sequence (as for our sample), the errors are relatively large, particularly if there is a significant uncertainty in stellar parameters. By applying an upper limit to the distance, we confine this technique to stars with accurate parallax measurements by *Hipparcos*, reducing the uncertainties in luminosity. We believe the largest source of observational uncertainty is the determination of spectral type. Table 1 lists the ages and the method used to determine them. The age estimate used in this study is listed first, with others included for comparison purposes. We have compared our H-R–derived age estimates with those from the literature where such are available, and we find that there are no substantial systematic differences, to the level that is necessary for the purposes of this study. This comparison is displayed on a star-by-star basis in Table 1 and summarized in the Appendix.

5. ANALYSIS

5.1. *Identifying* 24 μm *Excesses*

The large beam used for the *IRAS* measurements could result in false excesses due to a random background source lying too close to the star to be identified separately. To calculate the probability of this type of coincidence, we used the 25 μm source density on the sky as measured by *IRAS* in two 5° radius fields, placed, respectively, at the north and south Galactic poles. We found that the probability of one chance coincidence in our entire *IRAS*-derived sample is about 3%. Therefore, we have made no corrections for such coincidences. Gorlova et al. (2004) analyze the probability of chance coincidences within the much smaller MIPS point-spread function (diameter 6″) in the cluster M47, again finding that they are unlikely. A similar conclusion should hold for the other clusters used in our study. The field stars measured with MIPS are substantially brighter than the cluster members, and hence confusion is even less of a possibility with them.

Extinction is also not a significant issue in this work. All of our sample stars are unobscured, or very lightly obscured ($A_V < 0.3$). The extinction differential between K and [24] is only 10% of A_V, while the differential between J and K is 17% of A_V (Rieke & Lebofsky 1985). Thus, even at the maximum extinction levels, the effects are no larger than the measurement errors.

To determine the level of excess emission at 24 μm (Table 1, col. [7]), we used an empirical, self-calibrating approach rooted in traditional stellar color photometry. We assumed that the intrinsic, photospheric $K - [24]$ (or $K - [25]$ for the *IRAS* targets) colors for the photospheres of all the stars in the sample were identical. We computed the observed colors from the current calibrations but introduced a normalizing constant for each of the MIPS and *IRAS* photometry sets, such that the mode of the resulting color histograms occurred at 1.00. There was no dependence of the mode on stellar age, demonstrating that our procedure was not hiding small excesses for young stars. For the MIPS data the half-width about the mode of the distribution was 3%–4%; it was about twice that for the *IRAS* data. These values are in agreement with the estimated errors in the K-band and 24/25 μm photometry. However, there are a number of large-amplitude negative outliers, up to ~20%, for both *Spitzer*- and *IRAS*-measured stars. These cases may be related to errors in the near-infrared photometry, to source variability, or to the effects during scan-map observations of small specks of dirt on the instrument pick-off mirror.

We associate the narrow peak in the distribution of colors to be from the stars with no significant 24 μm excess and conclude that stars with a ratio greater than the mode by ~15% for the MIPS data or ~25% for the *IRAS* data have significant excesses (at the 3–4 σ level, based on the distributions just described). To discuss the sample in a uniform fashion, in the following we use a threshold of 25% for identification of a significant excess.

To test the validity of this procedure, we used Kurucz stellar atmospheric models to extrapolate from visible and near-infrared photometry to 24 μm, concentrating only on a subset of stars with high-quality photometry as a foundation for the extrapolation. The behavior for these stars agrees well with that from our empirical approach: that is, a majority of the stars show similar small scatter around a purely photospheric excess ratio, and the two methods agree closely on the existence and amounts of excess emission that would be assigned. We did not apply the Kurucz model approach to our entire sample because the necessary high-quality photometry is not available. Furthermore, although the extrapolated model results can be shown to be consistent with the prelaunch estimates of instrument throughput to about 15%, such models have been used in refining the calibration beyond this level. Therefore, using the same models to test the A star calibration has some degree of circularity. In any case, the extrapolations showed slightly greater scatter than the empirical approach, indicating that inclusion of the shorter wavelength photometry and models was degrading the results. Thus, we consider the work reported here to be an important step toward improving the instrument calibration and our understanding of spectral extrapolations based on theoretical stellar atmosphere models.

5.2. *Trends in Amounts of Excess Emission*

The distribution of 24 μm excess with stellar age is illustrated in Figure 1. It shows a rapid decline in the maximum amount of excess; not plotted are HR 4796A and β Pic, which are both well off the top of the vertical scale (their ages are indicated by upward-pointing arrows). Because they are very young, it is

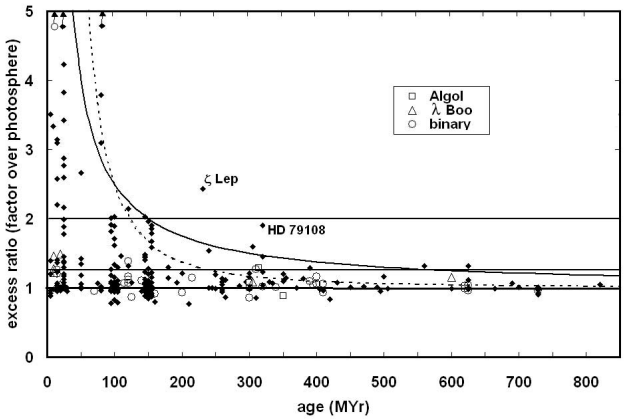

FIG. 1.—24 μm excess vs. age. Excess emission is indicated as the ratio of the measured flux density to that expected from the stellar photosphere alone: a value of 1 represents no excess. Additional horizontal lines show the threshold for detection of an excess, 1.25, and the one for a "large" excess, 2. The upward-pointing arrows are, from left to right, HR 4796A, β Pic, and HD 21362. The thin solid line is an inverse time dependence, while the thin dashed line is inverse time squared. Age uncertainties are generally factors of roughly a factor of 1.5 below 200 Myr (where ages are almost entirely from cluster and moving group membership) and roughly a factor of 1.5–2 above 200 Myr (where many ages are assigned by placing the stars on the H-R diagram).

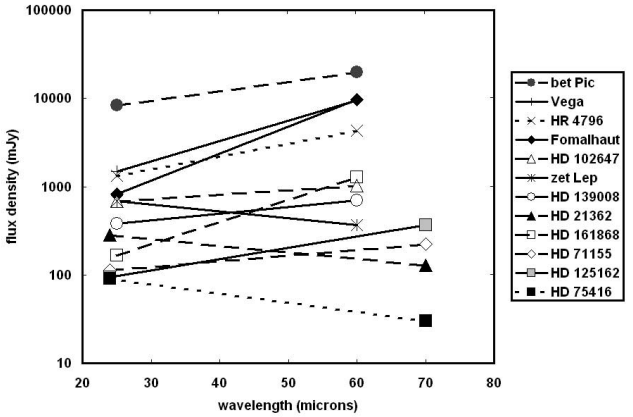

FIG. 2.—Slopes of debris disk SEDs. Data are from *IRAS*, 25 to 60 μm, or MIPS, 24 to 70 μm. Stars less than 25 Myr old are shown as dotted lines, between 25 and 200 Myr as dashed lines, and older than 200 Myr as solid lines.

possible that their large excesses are associated with a transitional stage from protoplanetary disks into true debris systems. Other stars in the youngest age range may also be in this transitional stage. None of the conclusions of this paper depend on the exact phase of activity in these stars.

Although it is substantially older, HD 21362 is also off the top of the figure. It has strong 24 and 70 μm excess, but with a "hot" spectral energy distribution (SED) as shown in Table 2 and Figure 2. The behavior of the other systems qualitatively agrees with previous work suggesting a decline of debris disk activity with stellar age (e.g., Habing et al. 2001; Decin et al. 2003). As indicated in Figure 1, the upper envelope of the excesses can be fitted roughly by t_0/t, with $t_0 \sim 150$ Myr. The timescale of the decay is uncertain because of the age uncertainties. By redrawing Figure 1 for a variety of realizations of the age distribution randomly varied by a factor of 2 uncertainty for each star, we conclude that t_0 lies between 100 and 250 Myr. A decay of the upper envelope as fast as the inverse of time squared can be ruled out because of the persistence of excesses beyond ages of 200 Myr. In addition, an interesting new result (previously suggested by Spangler et al. [2001] and Decin et al. [2003] but established in detail here) is the large variety of excess amounts at any given age.

Table 3 groups the observations into bins in age and amount of excess. The table indicates that more than 10% of the stars older than 190 Myr have 24 μm excesses. However, four of the 10 stars with indications of excess (HD 12216, HD 56537, HD 87696, and HD 122408) have excess ratios between 1.26 and 1.32 based on moderate S/N detections in the *IRAS* FSC. These measurements need to be confirmed. The excesses in the remaining six are all detected at substantially higher confidence levels and five of them have confirming measurements of excesses at 60 or 70 μm (the exception is HD 178253). We conclude that at least 7% of the stars in our sample older than 190 Myr have significant 24 μm excesses.

We selected the bins in Table 3 to search for rapid evolution in disk emission. However, there is no statistically significant difference in the grouping for ages of less than 10, between 10 and 24, and between 25 and 90 Myr. We therefore combine these three age bins and also combine the excess bins into three that illustrate clearly the overall behavior, and display the result in Figure 3. We find that about 50% of the stars have no excess

TABLE 3
EXCESSES VS. AGE

Excess Ratio	<10 Myr	10–24 Myr	25–89 Myr	90–189 Myr	>190 Myr
<1.25	5	11	23	80	75
fraction	0.56	0.52	0.53	0.74	0.88
1.25–1.39	0	3	4	7	6
fraction	0	0.14	0.09	0.06	0.07
1.4–1.99	1	2	5	17	3
fraction	0.11	0.10	0.12	0.16	0.04
2–2.99	0	2	5	4	1
fraction	0	0.10	0.12	0.04	0.01
3–5	2	2	5	0	0
fraction	0.22	0.10	0.12	0	0
>5	1	1	1	0	0
fraction	0.11	0.05	0.02	0	0

NOTES.—The primary entry is the number of stars in each category of age and excess fraction. Under that entry, we give the fraction this number of stars represents of all the stars in the age range. In judging the significance of variations, one should take into account the statistical weight of these fractions implied by the number counts.

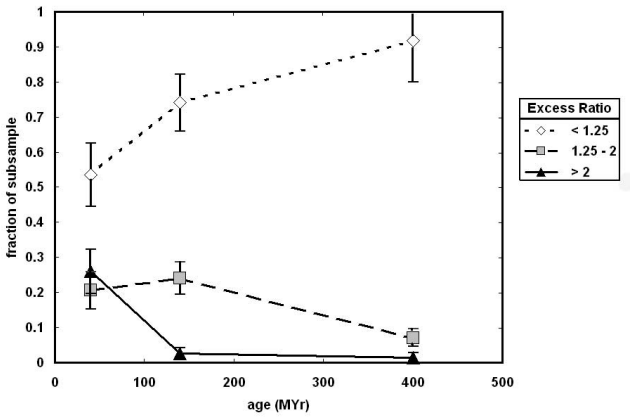

FIG. 3.—Trend of excess with age, based on the statistics in Table 2.

in the lowest age interval, rising to ~90% for the stars of age 190 Myr or greater. The portion of stars with excesses equal to or greater than the 24 μm photospheric emission (hence with excess ratios of 2 or more) decays rapidly from about 25% in the lowest age bins to only one star (1%) for the stars of age 190 Myr or greater. We have used the binomial distribution to estimate the significance of the apparent change in proportion of stars with excess ratios larger than 2. There is only a probability of 2×10^{-7} that the two sets of observations (0–90 and >190 Myr) are drawn from the same distribution. Because the youngest stars (<10 Myr) have the same distribution over excess ratios as those between 10 and 90 Myr old, this result cannot arise from the contributions of stars in transition between protoplanetary and true debris disks. The trend for intermediate levels of excess ratio, between factors of 1.25 and 2, is for a slower decay, from 22% for the youngest grouping to a third of this value for the oldest. The probability that the youngest and oldest groups are drawn from the same distribution for this excess ratio range is less than 10^{-2}, but given the uncertainties in excess ratios for the stars observed with *IRAS* as discussed above, the significance of the change is less than indicated by this statistic.

A variety of previous studies have attempted to determine the duration of the debris-disk phenomenon (e.g., Habing et al. 2001; Spangler et al. 2001; Haisch et al. 2001; Laureijs et al. 2002; Decin et al. 2003; Mamajek et al. 2004; Liu et al. 2004, and references given in these articles). From these works, it is apparent that disk clearing occurs from the inside outward. Simple radiative equilibrium suggests that the 24 μm excesses arise in a zone extending roughly from ~10 to 60 AU from the A stars in our sample, which corresponds to a temperature zone similar to the region of giant planet formation in the solar system. The clearing is much faster for the interior zones (Haisch et al. 2001; Mamajek et al. 2004), e.g., a few million years for the region of protoplanetary disks that radiate at 3.6 μm (Haisch et al. 2001). The clearing time for the outer zones of debris disks observed in the submillimeter appears to be roughly consistent with what we find at 24 μm, that is, inversely with time and with a characteristic time of the order of 150 Myr (Liu et al. 2004). Figure 3 suggests also that the decay time is distinctly different for different degrees of excess, a result that may correlate with different stages in planet building around these stars. For example, the behavior might correlate with current ideas for the evolution of the solar system (e.g., Chambers 2004), where there is a period of 100–200 Myr when large, planet-sized bodies occasionally collide, followed by continued collisions between asteroid-sized objects.

TABLE 4
EXCESSES VS. ROTATION RATE

Name (1)	Excess Ratio (2)	Age (Myr) (3)	$v \sin i$ (4)
Fast-rotating Stars			
HD 21362	8.37	80	385
HD 23753	1.08	125	258
HD 23923	2.15	125	307
HD 87901	0.95	140	353
HD 133880	0.99	15	350
HD 133937	0.95	15	350
HD 135742	1.03	100	230
HD 145964	1.20	5	295
HD 214923	1.16	120	210
Probable Slow-rotating Stars			
HD 23642	1.38	125	37
HD 23964	1.17	125	16
HD 33904	1.03	150	14
HD 34868	0.96	100	97
HD 38206	3.34	9	30
HD 48915	0.95	70	5
HD 80950	3.79	80	40
HD 123445	1.04	15	66
HD 144661	0.96	5	72
HD 188228	0.98	10	85
P1165	1.00	100	65

Most of the previous studies have assumed that the decay of infrared excess proceeds in a continuous fashion from similar initial conditions for all stars and can be characterized roughly by a single time constant. In a review of previous work, Decin et al. (2003) pointed out that there is a large spread in infrared fractional luminosity at any given age. The far more extensive data in our study confirm this conclusion. A result from our study that appears not to be anticipated by previous work is that a large fraction (up to ~50%) of even quite young stars have small, perhaps nonexistent, excesses at 24 μm.

Another possibility is that the nature of circumstellar disks is related to the stellar rotation. Unfortunately, although an observation of rapid rotation is unambiguous, a star observed to have slow rotation may actually be rotating slowly, or it may be a fast rotator seen pole-on. In Table 4, we list stars with ages $\leq$150 Myr, divided into those with $v \sin i > 200$ and less than 100 km s^{-1}. The distributions of excesses are indistinguishable. However, because the number of stars is small, we can only tentatively conclude that the debris disk behavior is not strongly related to rotation.

Figure 1 illustrates another aspect of the behavior of these stars. We have plotted with separate symbols Algol-type systems, other binaries, and λ Boo stars. Although the number of examples is small, it appears that none of the three attributes leads to large excesses—in fact, one can argue that binarity may promote smaller than typical excess. One outstanding exception is HR 4796A, with a huge excess; maybe this behavior arises because of this star's youth and the possible transitional nature of its circumstellar disk. Alternatively, the binary separation is large, so the companion may not affect the disk properties.

All of these second-order effects on the incidence and longevity of debris disks can be investigated in more detail with

additional data being obtained both in our program and in others using *Spitzer*.

6. DISCUSSION

The behavior of the 24 μm excesses should give us new insights to planet formation around these stars. The behavior is subject to two bounding cases: (1) the large variety in amounts of excess reflects intrinsic variations in the circumstellar disks that evolve in a continuous fashion from different starting conditions; or (2) the disks are all fundamentally similar, and the variety results from a high degree of variability due to large collisions and the resulting short-term increases in the density of small grains around the stars. We discuss each of these possibilities in turn. We find that a bit of each of the bounding conditions is required to explain the data.

6.1. *Do Debris Disks Have Large Intrinsic Differences?*

We believe the data favor significant intrinsic differences among debris disks, for the following reasons.

One of the most important results of our work is that up to $\sim$50% of the youngest stars in our sample do not have significant excesses at 24 μm, as shown in Table 3. This result appears to hold even down to the youngest ages that we can probe, stars less than 10 Myr old. Given the timescale for giant planet formation and migration and the expected resulting chaos in a debris disk, the stars with no excess emission at earlier than 10 Myr would have to go through these steps surprisingly quickly to agree with the observations. In contrast, we observe very slow fading of intermediate-sized excesses, as shown in Table 3 and Figure 3. If all the disks are similar, how can we reconcile 50% of the disks evolving to below our detection limit in less than 10 Myr, but 25% still being detectable at 150 Myr? These issues can be avoided if there is relatively little material in the 24 μm–emitting zone around some of these stars immediately after the protoplanetary disks have cleared.

Some evidence for a subset of young stars having weak disk signatures comes from Haisch et al. (2001), who find that even at $\sim$0.5 Myr, 16% $\pm$ 8% of young stellar objects have no excess at 3.6 μm. However, the region probed at this wavelength lies far inside the region we probe at 24 μm. Another determination can be made from the ISOCAM measurements in ρ Oph (Bontemps et al. 2001), which extend to 14.3 μm and therefore probe close to the region we observe at 24 μm. From their compilation (their Tables 3 and 4), we have selected a subsample of objects with $L \geq 1\ L_{\odot}$, both to guarantee completeness and cluster membership and to include stars with masses probably $\geq 1\ M_{\odot}$. Of 17 total objects of Class II and III, six have spectral slopes ≤ -2 between 2 and 14 μm, where a slope of -3 is for a hot blackbody. This proportion is slightly lower but similar to the 15/29 A stars less than 25 Myr old in our sample that show no significant excess emission. The ρ Oph young stellar objects appear to be less than 1 Myr old (e.g., Luhman & Rieke 1999). Similarly, of 12 objects in Cham I with appropriate data and luminosity greater than 1 $L_{\odot}$, four are designated as Class III (no substantial excess between 2 and 14 μm) by Persi et al. (2000). This behavior supports the possibility that a significant portion of the stars with no significant debris disk emission in our A star sample are stars that quickly lost their protostellar disks in the region of interest.

Further support for the possibility that some stars divest themselves of circumstellar disks very early in their lives comes from submillimeter observations. For example, Duvert et al. (2000) report upper limits to CO ($J = 2$–1) emission from 11 of 12 weak-lined T Tauri stars corresponding to upper limits of $\sim 6 \times 10^{-7}\ M_{\odot}$ for the mass in gas in any circumstellar disks, along with continuum upper limits at 1.3 mm, corresponding to a upper limits of $\sim 2 \times 10^{-4}\ M_{\odot}$ in the disk. These values are significantly below estimates of the disk mass of $\sim$0.01 $M_{\odot}$ thought to be required to form a system like the solar system (e.g., Carpenter 2002).

6.2. *Is Debris Disk Emission Dominated by Large Events?*

Debris disks must be maintained by continuous collisional processes, which makes it plausible that their properties at any one time may differ because of recent, major collisions between large planetesimals.

For example, Kenyon & Bromley (2004) calculate numerically that the clearing time for the 20 μm flux due to a collisional cascade in a debris disk is about 1 million years. Dominik & Decin (2003) compare collisional cascade clearing times using an analytic approach, finding a typical timescale of a few tens of millions of years at large radii (50 AU), decreasing as the 1.5 power of radius. Alternative mechanisms that may act to clear particles from these disks are photon pressure for sizes below about 10 μm (which acts nearly instantaneously) and Poynting-Robertson drag for sizes between 10 and 100 μm (which decays as inverse time squared; Dominik & Decin 2003). For all these mechanisms, the appropriate clearing timescale for particles in the 24 μm–emitting zone is no more than 1–10 million years.

Thus, the debris disks in virtually all of our stars need to have been replenished by recent planetesimal collisions, which will create new objects on collision orbits to initiate new collisional cascades and produce additional debris. This process will remain active throughout the period of major planet building and orbital migration. Estimates for the first steps of these processes range around a few million years (Cionco & Brunini 2002; Rafikov 2003; Chambers 2004). The accretion end game is predicted to be dominated by a small number of collisions between large bodies (e.g., the early Earth and the impactor that caused formation of the Earth's Moon) and may stretch over 100–200 million years (Chambers 2001). Even afterward, collisions between smaller bodies will continue and will trigger new collisional cascades that will inject new dust into debris disks, but at a more modest level.

During the accretion end game, we might expect that debris disks would be dominated by major collisions and hence that there could be substantial variation in their properties. In fact, there is a substantial range of properties among well-known debris disks. As an example, we compare Vega, Fomalhaut, and ζ Lep. All three stars are of very similar mass and age. The first two have very similar SEDs, with modest excesses at 24 μm, rising steeply to 60/70 μm (Tables 1 and 2, Fig. 2). Despite this similarity, their images are dramatically different. Fomalhaut is dominated by a circumstellar ring of radius $\sim$110 AU in the submillimeter, which is filled in at 24 μm. This structure suggests that warm dust grains are seen falling into the star (Stapelfeldt et al. 2004). Vega also shows a probable circumstellar ring of similar size to that of Fomalhaut in the submillimeter (Wilner et al. 2002). However, at 24 μm, it extends to a radius of $\sim$600 AU, far outside the submillimeter source. This structure suggests that small grains are being expelled from the system under radiation pressure (Su et al. 2005). In comparison, ζ Lep has a dramatically different SED, with a very large excess at 24 μm (see Fig. 1), but only a relatively modest excess at longer wavelengths (Fig. 2). Thus, the structure of its debris system

must include far less cold dust than is seen in the circumstellar rings around Vega and Fomalhaut. In agreement, most of the dust responsible for the 24 μm excess is tightly confined around the star, within a radius of 6 AU (Chen & Jura 2001).

Evidence for the variety of debris disks can be extended to other systems, including those too far away to resolve, by use of SEDs. Figure 2 shows the spectral slopes from 24/25 to 60/70 μm for 12 systems, all selected to have substantial excesses at 24 or 25 μm. If these systems were all fundamentally similar, we would expect that the SEDs within a given age range would resemble each other, and that there would be an evolutionary change of SEDs from one age range to the next. Instead, there is a broad variety in each range, with no apparent trend.

The large variety of behavior in Figure 2 suggests variability in disk properties due to major collisional events, because it would otherwise require huge differences in disk structure to be maintained for hundreds of millions of years. We consider a few individual cases to probe this possibility in more detail.

ζ Lep.—The small size of the debris system, under 6 AU in radius (Chen & Jura 2001), results in very rapid dust removal; Dominik & Decin (2003) show that the relevant processes operate on timescales proportional to the 1.5 to 3.5 power of the distance of the debris from the star. The timescales are all less than 10 Myr for this system. Moro-Martín & Malhotra (2002) show that planets only slightly slow the dust removal. The stellar age of 230 Myr therefore spans many replenishment timescales, if the system has remained in an equilibrium similar to its current appearance. Moro-Martín et al. (2005) show that the influence of planets on a debris disk SED is invariably to remove flux in the 10–40 μm region and to produce a relatively cold spectrum. The hot SED of ζ Lep (see Fig. 2) is not consistent with this prediction. Thus, if the ζ Lep has maintained its current appearance for the life of the star, it must have no major planets to help maintain or replenish the system and must have sustained it through a large number of replenishment times, an unlikely set of conditions. A recent collision that injected a large amount of dust into the system is a more likely possibility.

HD 21362 and HD 71155.—These stars have relatively "hot" SEDs, like that of ζ Lep, and are likely to pose similar problems for equilibrium models.

Vega.—It requires a very large generation rate for small grains to play a major role in the radiometric signature of a debris disk, because they are ejected quickly by photon pressure. Nonetheless, the appearance of the Vega system at 24–160 μm is dominated by such grains (Su et al. 2005). If the large production rate were the result of an equilibrium collisional cascade, we would expect to see a similar effect in Fomalhaut, which is a virtual twin of Vega in luminosity, age, the SED of its debris disk, and in the structure observed in the submillimeter. Since there is no evidence of small grains outside the 110 AU radius circumstellar debris ring in Fomalhaut, we conclude that the Vega small grains are more likely to be the result of a recent event rather than an equilibrium product of its debris system.

β Pic.—As with Vega, the large extent of this system near 10 μm requires the presence of very small grains, being ejected by radiation pressure (Augereau et al. 2001). Given their short dwell times in the system, the most plausible explanation for their existence in sufficient numbers is that they are the product of recent collisional processes.

6.3. *Theoretical Results and Comparison with the Solar System*

A number of theoretical studies of the solar system suggest that large events play a central role in producing episodic generation of dust, and therefore support the hypothesis that the disk signatures in the A stars are influenced significantly by individual, large events. These studies reflect conditions within an overall context in which there is rapid evolution for the first few million years as embryo planets form and large planets undergo orbital migration. For the following 100–200 Myr, the planetary accretion end game is dominated by occasional huge collisions between planet-sized bodies (Chambers 2001, 2004), such as the one responsible for the formation of the Earth's Moon.

In these studies, dust production begins with collisions between bodies typically kilometer-sized or larger, analogous to asteroids or comets. Roughly speaking, the amount of dust in a system is related to the supply of such large bodies or, equivalently, the total mass of the planetesimal disk. The dust evolution timescale is governed partly by the overall decline in the number of large bodies in the system over time, but also by the rate at which dust is removed. Dominik & Decin (2003) calculate the rates of large body collisions and of dust removal analytically. The number of large bodies (the mass of the disk) decreases as t^{-1}, while the rate of dust production (which goes as the number of colliders squared) drops off more steeply, as t^{-2}. The time dependence of the amount of dust depends on the physical mechanism for its removal. For the most tenuous disks (those with masses $\lesssim 10^{-3}\ M_{\oplus}$ for Dominik & Decin's standard parameters), Poynting-Robertson drag acts to clear out dust from the system. In this regime, where the removal process is linear with the amount of dust present, the dust mass declines as t^{-2}. For more dense disks ($\gtrsim 10^{-3}\ M_{\oplus}$) collisions between dust particles become more frequent and start to dominate the dust removal. In this regime, the removal process goes as the square of the amount of dust present, resulting in a dust mass decline as t^{-1}. Based on the characteristics of disks detected via infrared excess, in particular their fractional luminosity, Dominik & Decin argue that these disks are massive enough to fall in the collisional regime, such that the observed infrared emission should fall off as t^{-1}. They determine a timescale for this overall dust evolution on the order of 100 Myr for the outer part of the zone probed at 24 μm, and an order of magnitude less for the inner part of the zone.

However, numerical simulations of the solar system show that there is a second, faster timescale also applicable to debris disk evolution. Durda & Dermott (1997) improved on the general collisional cascade described by Dohnanyi (1969) by considering variations in the internal strength of the parent bodies and specifically matching their results to the known distribution of asteroids. In addition, rather than relaxing to an analytic equilibrium, they followed the time evolution due to stochastic events. Grogan et al. (2001) expanded on this work and have produced evolutionary plots of the asteroidal dust surface area over the entire lifetime of the solar system. They find sudden increases of up to an order of magnitude, followed by a short dust decay timescale of several Myr. These events are superimposed on the long slow decline of dust that must occur as mass is continually lost from the system.

Kenyon & Bromley (2004) have carried out detailed numerical simulations of the time dependence of debris disk excess emission at 20 μm in a young solar system, concluding, "As the 10–20 μm excesses decline, individual collisions among 10–1000 km objects produce fluctuations in the dust production rate. These disruptive collisions yield large variations in the 10–20 μm excesses." Specifically, their simulations show events that boost the flux density of the disk by factors of $\sim$3 above the 1/time decline of the overall collisional cascade.

The model of Grogan et al. (2001) of the solar system's asteroid belt (see particularly their Fig. 19) shows that the baseline total area of the belt decreases gradually over the age of the solar system by a factor of ~10. On top of this long, gradual decay are seen many discrete events that are produced by collisions of individual asteroids. Each collision-derived event decays with a timescale of roughly several 10^6 yr. These simulations indicate that the dust surface area in the asteroid belt was at greater than twice of its quiescent level (i.e., the slowly decaying baseline) for 10% of the time, even after four billion years of evolution. Since the total area and the expected debris-disk emission are closely related, the overall picture of the infrared emission of the zodiacal belt is that it has decreased over 4.5 Gyr gradually, but with numerous spikes that provide a ~10% duty cycle in a "high" state.

This theoretical modeling of the dust produced by individual collisional cascades is supported by observations of dust in the asteroid belt. Inclined dust bands observed by *IRAS* within the 25 μm zodiacal emission trace residual dust thought to be created in collisional cascades initiated by relatively recent collisions of asteroids (Low et al. 1984; Sykes & Greenberg 1986). In particular, the $i = 2\overset{\circ}{.}1$ dust bands have been attributed to the collisional breakup of a $\gtrsim$25 km asteroid just 5.8 Myr ago, the remnants of which can still be seen today as the Karin cluster (Nesvorný et al. 2002). Dermott et al. (2002) and Nesvorný et al. (2003) show that the $i = 10^\circ$ band is probably a result of the breakup of the Veritas asteroid family precursor about 8.3 Myr ago, an object thought to be ~140 km in diameter. They calculate that dust associated with this event still accounts for ~25% of the thermal emission from the zodiacal cloud, even after 8 Myr of dust destruction. Extrapolating back to the time of the breakup, the emission of the zodiacal cloud would have been dominated by this event at the time it occurred (as indicated in eq. [2] of Dermott et al. 2002).

The age since these events is consistent with the theoretical modeling described above and strengthens the conclusion that individual events can dominate the amount of dust within a system over megayear timescales.

The overall evolution of dust in a debris disk is therefore likely to be a combination of the long and short dust-production timescales—short bursts in activity as spikes on top of the long overall decay. The A star data presented here can be interpreted as observational evidence for this type of model operating around many of these stars. We suggest that for A stars that have disks, the overall disk masses (and hence area and dust mass) decrease gradually over time, with a timescale of $\sim 10^8$ yr. However, at any given epoch, a disk can have recently suffered a dust-producing collision that increases its brightness by an order of magnitude.

A stars that we observe to have no excess could merely be in a "quiescent" stage (no recent collisions) in which the disk surface area is governed only by its long-timescale decay baseline. However, it seems likely that many of these stars belong to a population that reached the debris disk stage, at ~5 million years of age, with most of the material in the 10–60 AU range already dissipated.

7. CONCLUSIONS

We have combined *Spitzer, IRAS*, and *ISO* observations of individual field stars and of open cluster members to document the evolution of debris-disk infrared excesses at 24 μm around stars of about 2.5 $M_\odot$. We find the following:

1. A large fraction (up to ~50%) of young stars have small or nonexistent 24 μm debris-disk excesses.
2. The fraction of stars with large excesses (more than a factor of 2 relative to the photosphere) at 24 μm decreases significantly by an age of ~150 Myr.
3. Intermediate excesses (factors of 1.25–2) decrease much more slowly and are exhibited by a significant fraction (~7%) of these stars even at several hundred megayears of age.
4. Within the limited statistical significance we can achieve with this sample, large excesses do not appear to be associated with Algol-type systems or other types of binaries, or with λ Boo stars. In fact, binary stars may tend to have smaller excesses than single stars.

When we combine the statistical results from this sample with observations of individual stars such as Fomalhaut, Vega, and ζ Lep, we conclude the following:

5. From the rapid appearance of many stars with little 24 μm excess, combined with the slow decay of the intermediate-level excesses, it appears likely that there are substantial intrinsic differences among the debris disks around these stars.
6. From the variety of debris disk behavior observed in individual stars, it appears that we are also seeing the results not just of disk differences, but also of variable behavior, where a single large planetesimal collision can dominate the debris-disk properties until its residue is cleared from the system. This behavior agrees generally with what we know about the evolution of the solar system, and also with theoretical models of planetary system formation.

We thank Christine Chen, Chris Corbally, and Amaya Moro-Martín for helpful discussions. This research made use of the SIMBAD database, operated at CDS, Strasbourg, France. This publication also makes use of data products from the Two Micron All Sky Survey, which is a joint project of the University of Massachusetts and the Infrared Processing and Analysis Center/California Institute of Technology, funded by the National Aeronautics and Space Administration and the National Science Foundation. Support for this work was provided by NASA through contract 960785 issued by JPL/California Institute of Technology.

APPENDIX

AGE DETERMINATION FROM THE H-R DIAGRAM

The first step in determining stellar ages from placement on the H-R diagram was to gather a consistent set of classification data. Parallaxes for all the stars in question are available from *Hipparcos*, and since the stars are all relatively close, the accuracies are generally 10% or better. We preferentially took spectral types from Gray et al. (2004). We also took temperatures from this reference when they were available. However, types for most of the stars were not available from this source, and in these cases we took types directly from the recommended values in the SIMBAD database.[5] For these stars, we used a spectral type to temperature conversion

[5] See SIMBAD Web site: http://simbad.u-strasbg.fr/Simbad.

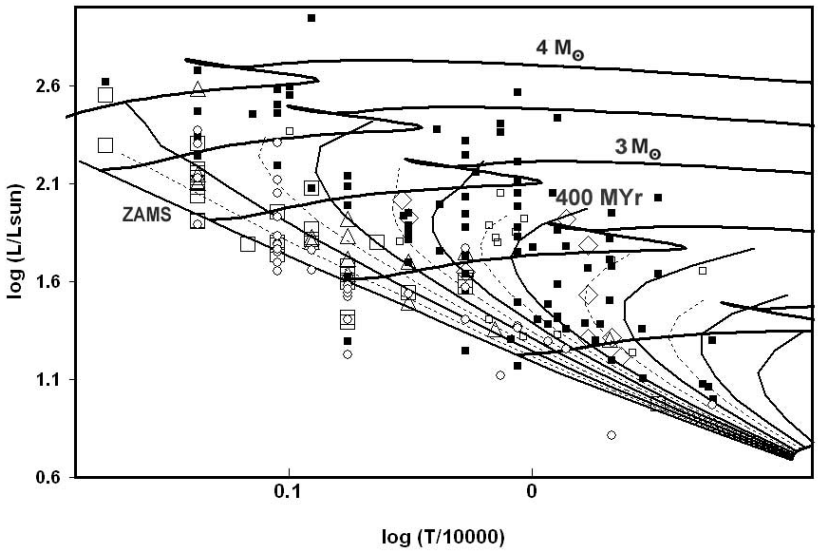

FIG. 4.—H-R diagram with program stars. Heavy solid lines show evolutionary tracks at 1.5 $M_{\odot}$ (*bottom right*), 2, 2.5, 3, 3.5, and 4 $M_{\odot}$ (*across the top*). Time steps are shown at the zero-age main sequence (*light solid line running from top left to bottom right*), 50 Myr (*dashed line*), 100 Myr (*solid line*), 150 Myr (*dashed line*), 200 Myr (*solid line*), 250 Myr (*dashed line*), 300 Myr (*solid line*), 350 Myr (*dashed line*), 400 Myr (*solid line*), 500 Myr (*dashed line*), 600 Myr (*solid line*), 700 Myr (*dashed line*), and 800 and 1000 Myr (*solid line*). Large open boxes show stars from our sample with ages from cluster and moving group membership that are less than 80 Myr. Open circles show additional members of the U Sco association with an age of ~5 Myr. Open triangles show stars from our sample with ages between 80 and 200 Myr, and open diamonds show stars with ages greater than 200 Myr, all determined from cluster and moving group membership. Small open squares represent ages from the literature. Small filled squares represent program stars for which we used location on the H-R diagram to estimate ages.

from Gray & Corbally (1994), which defines a system that is consistent with that used by Gray et al. (2004). We preferred to base stellar luminosities on infrared photometry because it removes any concerns about extinction and reduces the effects of metallicity. For most of the stars, we were able to obtain accurate near-infrared photometry from the references listed in Table 1. In a few cases in which the star was bright enough to saturate the 2MASS survey and no other high-quality photometry was available, we used visual photometry from the SIMBAD database, standard colors, and *IRAS* band 1 (12 μm) observations as surrogates for near-infrared data. We used the *K* photometry when available, or visual photometry, for luminosity determination. In all cases, we then made bolometric corrections to total luminosities (Lang 1986), using stellar colors from Tokunaga (2000) and Kidger & Martín-Luis (2003).

To convert the H-R diagram placements to stellar age, we used the Y2 isochrones from Yi et al. (2003). The issues in matching such isochrones to stellar characteristics are discussed by Song et al. (2001). In our case, where distances are well determined, the most important random observational uncertainties are due to errors in assigning spectral types and the resulting temperatures. In addition, stellar rotation modifies the evolutionary rates and the apparent luminosities and temperatures, and can make these latter two parameters dependent on the orientation of the star toward the observer. Since it is impossible to tell, for example, whether a star is a true slow rotator or appears to be one because we view it pole-on, rotational effects represent an unavoidable source of systematic error in such age determinations.

When the Y2 isochrones were plotted on the H-R diagram with the stars of our sample, we found that they did not match the zero-age main sequence defined by the stars indicated to be less than 50 Myr old from cluster and moving group measurement, and that there was a disproportionate number of stars in the region of fast evolution toward the giant branch. The discrepancies may be due to a variety of the error sources discussed above, particularly stellar rotation. We made an empirical correction by reducing the temperature scale for the isochrones by 8%, an adjustment consistent with the expected overall effects expected from rotation. The resulting H-R diagram is shown in Figure 4. A number of stars fall in a "negative age" regime, probably because of errors in spectral types.

The ages we estimate are compared with other determinations in Table 1, where for all dwarf stars with parallaxes $\geq$15 mas and with ages determined in other ways, we list also the age we estimate from the H-R diagram technique. The agreement is generally within a factor of 2, usually better. As a further consistency check, we compare the ages determined by us from the H-R diagram in Figure 4 with the measurements of Song et al. (2001) using Strömgren photometry (and with a number of other differences in approach). The result is shown in Figure 5. There is generally agreement within the errors. In particular, the diagram makes it clear that the disagreements are centered on stars for which both techniques have large errors. The two discordant stars, Fomalhaut and β Leo, are in regions in the H-R diagram where there is little sensitivity to age, which probably affects the accuracy of the comparison estimates from the literature as well as those we make. There is no systematic difference between the two approaches. Figure 5 also shows ages from other approaches, many of which are given without error estimates and hence we have plotted them without error bars. Again, there is rough agreement with the ages from Song et al. (2001) and our determinations.

Because we forced agreement between the isochrones and observations for young stars, and we obtain reasonable agreement with both cluster/moving group ages and those of Song et al. (2001) for older stars, we accept the age determinations as being satisfactory for our purposes. In the end, we find that the debris disk behavior appears not to be a strong function of age beyond 200 Myr.

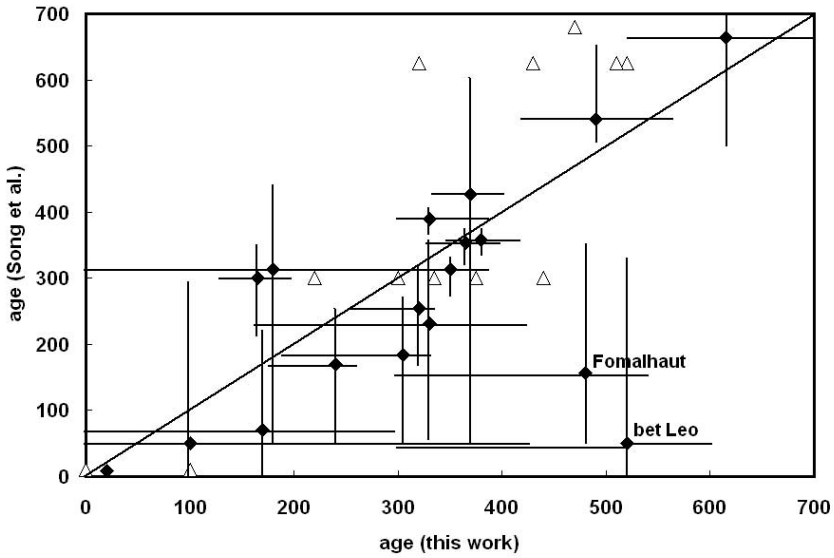

FIG. 5.—*Filled diamonds*: Comparison of stellar ages from this work, using the H-R diagram (Fig. 4), with ages from Strömgren photometry derived by Song et al. (2001). Error bars are estimated from the position on the H-R diagram for our ages, and as given by Song et al. Open diamonds compare ages obtained by other means; since errors are often not quoted, we do not show error bars on these points.

Therefore, the underlying reason our results are robust to age determination errors is that the great majority of stars for which we made age estimates from the H-R diagram are in the older than 200 Myr region, as shown in Figure 4. The separation of these stars from the younger ones where we have cluster- and moving-group-based ages provides an empirical confirmation that the former group is substantially older than the latter one.

REFERENCES

Augereau, J. C., Nelson, R. P., Lagrange, A. M., Papaloizou, J. C. B., & Mouillet, D. 2001, A&A, 370, 447
Aumann, H. H., et al. 1984, ApJ, 278, L23
Backman, D. E., & Paresce, F. 1993, in Protostars and Planets III, ed. E. H. Levy & J. I. Lunine (Tucson: Univ. Arizona Press), 1253
Barrado y Navascués, D., Stauffer, J. R., Hartmann, L., & Balachandran, S. C. 1997, ApJ, 475, 313
Barrado y Navascués, D., Stauffer, J. R., Song, I., & Caillault, J.-P. 1999, ApJ, 520, L123
Bonatto, Ch., Bica, E., & Girardi, L. 2004, A&A, 415, 571
Bontemps, S., et al. 2001, A&A, 372, 173
Cameron, L. M. 1985, A&A, 147, 47
Carpenter, J. M. 2002, AJ, 124, 1593
Carter, B. S. 1990, MNRAS, 242, 1
Chambers, J. E. 2001, Icarus, 152, 205
———. 2004, Earth Planet. Sci. Lett., 223, 241
Chen, C. H., & Jura, M. 2001, ApJ, 560, L171
Cionco, R. G., & Brunini, A. 2002, MNRAS, 334, 77
Cutri, R. M., et al. 2003, 2MASS All-Sky Catalog of Point Sources (Pasadena: IPAC)
Decin, G., Dominik, C., Waters, L. B. F. M., & Waelkens, C. 2003, ApJ, 598, 636
Dermott, S. F., Keoe, T. J. J., Durda, D. D., Grogan, K., & Nesvorý, D. 2002, in Proc. Asteroids, Comets, Meteors, ed. B. Warmbein (ESA SP-500; Noordwijk: ESA), 319
de Zeeuw, P. T., Hoogerwerf, R., deBruijne, J. H. J., Brown, A. G. A., & Blaauw, A. 1999, AJ, 117, 354
Dohnanyi, J. W. 1969, J. Geophys. Res., 74, 2531
Dominik, C., & Decin, G. 2003, ApJ, 598, 626
Durda, D. D., & Dermott, S. F. 1997, Icarus, 130, 140
Duvert, G., Guilloteau, S., Ménard, F., Simon, M., & Dutrey, A. 2000, A&A, 355, 165
Gerbaldi, M., Faraggiana, R., Burnage, R., Delmas, F., Gómez, A. E., & Grenier, S. 1999, A&AS, 137, 273
Gezari, D. Y., Pitts, P. S., & Schmitz, M. 2000, Catalog of Infrared Observations, ver. 5.1, http://ircatalog.gsfc.nasa.gov (Greenbelt: NASA)
Gordon, K. D., et al. 2005a, PASP, in press
———. 2005b, SPIE, in press
Gorlova, N., et al. 2004, ApJS, 154, 448
Gray, R. O., & Corbally, C. 1994, AJ, 107, 742
Gray, R. O., et al. 2004, NStars Spectra (Booue: Appalachian State Univ. Dark Star Obs.) http://stellar.phys.appstate.edu
Grogan, K., Dermott, S. F., & Durda, D. D. 2001, Icarus, 152, 251
Habing, H. J., et al. 2001, A&A, 365, 545
Haisch, K. E., Lada, E. A., & Lada, C. J. 2001, ApJ, 553, L153
Hauck, B., & North, P. 1993, A&A, 269, 403
Iliev, I. K., & Barzova, I. S. 1995, A&A, 302, 735
IPAC. 1986, *IRAS* Catalog of Point Sources, ver. 2.0 (Pasadena: IPAC)
Kenyon, S. J., & Bromley, B. D. 2004, ApJ, 602, L133
Kidger, M. R., & Martín-Luis, F. 2003, AJ, 125, 3311
King, J. R., Villarreal, A. R., Soderblom, D. R., Gulliver, A. F., & Adelman, S. J. 2003, AJ, 125, 1980
Lagrange, A.-M., Backman, D. E., & Artymowicz, P. 2000, in Protostars and Planets IV, ed. V. Mannings, A. P. Boss, & S. S. Russel (Tucson: Univ. Arizona Press), 639
Lang, K. R. 1986, Astrophysical Fromulae (2nd ed.; New York: Springer), 564
Laureijs, R. J., Jourdain de Muizon, M., Leech, K., Siebenmorgen, R., Dominik, C., Habing, H. J., Trams, N., & Kessler, M. F. 2002, A&A, 387, 285
Leggett, S. K., Bartholomew, M., Mountain, C. M., & Selby, M. J. 1986, MNRAS, 223, 443
Liu, M. C., Mathews, B. C., Williams, J. P., & Kalas, P. G. 2004, ApJ, 608, 526
Low, F. J., et al. 1984, ApJ, 278, L19
Luhman, K. L., & Rieke, G. H. 1999, ApJ, 525, 440
Mamajek, E. E., Meyer, M. R., Hinz, P. M., Hoffmann, W. F., Cohen, M., & Hora, J. L. 2004, ApJ, 612, 496
Moro-Martín, A., & Malhotra, R. 2002, AJ, 124, 2305
Moro-Martín, A., Wolf, S., & Malhotra, R. 2005, ApJ, in press
Moshir, M., et al. 1989, *IRAS* Faint Source Catalog, $|b| > 10$, ver. 2.0 (Pasadena: IPAC)
Nesvorný, D., Bottke, W. F., Dones, L., & Levison, H. F. 2002, Nature, 417, 720
Nesvorný, D., Bottke, W. F., Levison, H. F., & Dones, L. 2003, ApJ, 591, 486
Paunzen, E. 1997, A&A, 326, L29
Perryman, M. A. C., et al. 1998, A&A, 331, 81
Persi, P., et al. 2000, A&A, 357, 219
Rafikov, R. R. 2003, AJ, 125, 942
Randich, S., Pallavicini, R., Meola, G., Stauffer, J. R., & Balachandran, S. C. 2001, A&A, 372, 862
Rieke, G. H., & Lebofsky, M. J. 1985, ApJ, 288, 618
Rieke, G. H., et al. 2004, ApJS, 154, 25

Selby, M. J., Hepburn, I., Blackwell, D. E., Booth, A. J., Haddock, D. J., Arribas, S., Leggett, S. K., & Mountain, C. M. 1988, A&AS, 74, 127
Song, I. , Caillault, J.-P., Barrado y Navascués, D., & Stauffer, J. R. 2001, ApJ, 546, 352
Spangler, C., Sargent, A. I., Silverstone, M. D., Becklin, E. E., & Zuckerman, B. 2001, ApJ, 555, 932
Stapelfeldt, K. R., et al. 2004, ApJS, 154, 458
Su, K. Y. L., et al. 2005, ApJ, submitted
Sykes, M. V., & Greenberg, R. 1986, Icarus, 65, 51
Tokunaga, A. T. 2000, in Astrophysical Quantities, ed. A. N. Cox (4th ed.; New York: Springer), 143
Wilner, D. J., Holman, M. J., Kuchner, M. J., & Ho, P. T. P. 2002, ApJ, 569, L115
Yi, S. K., Kim, Y.-C., & Demarque, P. 2003, ApJS, 144, 259
Young, E., et al. 2004, ApJS, 154, 428